

Spin quantization axis dependent magnetic properties and x-ray magnetic circular dichroism of FePt and CoPt

I. Galanakis, M. Alouani, and H. Dreyssé

IPCMS-GEMME, 23, rue du Loess, F-67037 Strasbourg Cedex, France

We have performed a theoretical study of the magnetic circular dichroism in the x-ray absorption spectra (XMCD) of the equiatomic CoPt and FePt ordered alloys as a function of the spin quantization axis. We found that the magnetization axis is along the [001] direction and the magneto-crystalline anisotropy energy (MCA) for the FePt compound is twice as large as that of the CoPt compound in agreement with experiment. The band structure and the total density of states confirm that all electronic states contribute to the MCA, and not just the states at the vicinity of the Fermi level. The orbital magnetic moments decrease with respect to the angle between the [001] axis and the spin quantization axis, and are much larger for the CoPt compound. We show that the orbital moment anisotropy is reflected in the XMCD signal.

71.55.Ak, 78.70.Dm, 75.50.Cc

I. INTRODUCTION

The disordered equiatomic binary alloys of the XY (X= Fe, Co – Y= Pd, Pt) type crystallize in the fcc structure and the magnetization is along the [111] axis.¹ At low temperatures these alloys tend to order in the $L1_0$ layered-ordered structure and in this case the spontaneous magnetization tends to align perpendicular to the layer stacking explaining the behavior of CoPt films during the magnetic annealing.² The strong perpendicular magnetic anisotropy (PMA) is due to the highly anisotropic $L1_0$ structure and it makes them very attractive for magnetic recording devices.³ The latter structure can be also obtained by molecular beam epitaxy (MBE) of alternating layers of pure X and Y atoms due to the substrate induced constraints. The first observation of the $L1_0$ long-range order for a [001] CoPt film grown by MBE was made by Harp *et al.*⁴ in 1993 and for a [001] FePt film by Cebollada *et al.*⁵ Lately other techniques have been also employed to develop films presenting PMA. CoPt films were grown by sputtering by Visokay *et al.*⁶ and by evaporation by Lin and Gorman,⁷ and FePt films were grown by various sputtering techniques.^{8–12}

The magneto-crystalline anisotropy energy (MCA) can be probed by many techniques such as torque or ferromagnetic resonance measurements. Both these methods describe the MCA in terms of phenomenological anisotropy constants. It has been demonstrated by Weller *et al.*¹³ that x-ray magnetic circular dichroism (XMCD) is also a suitable technique for probing the MCA, *via* the determination of the anisotropy of the orbital magnetic moment on a specific shell and site. The x-ray absorption spectroscopy (XAS) using polarized radiation probes element specific magnetic properties of alloys by applying the XMCD sum rules to the experimental spectra.^{14–16} However for itinerant systems, in particular to low symmetry systems, the use of the sum rules is debated because they are derived from an atomic theory.^{15,17,18} Lately angle-dependent XMCD experiments have been used to provide a deeper understanding for the relation between MCA and the orbital magnetic moments.¹⁹

The x-ray absorption for CoPt multi-layers has been already studied experimentally by Nakajima *et al.*,²⁰ Koide *et al.*,²¹ Rüegg *et al.*,²² and Schültz *et al.*²³ Nakajima *et al.*²⁰ revealed a strong enhancement of the cobalt orbital moment when PMA was present, Koide *et al.*²¹ showed that with decreasing cobalt thickness the easy axis rotates from in-plane to out-of-plane, and Rüegg *et al.*²² that platinum polarization increases also with decreasing cobalt thickness. Hlil *et al.*²⁴ showed by x-ray absorption spectroscopy that modifications of platinum edges in different compounds are correlated to the change in the number of holes.

Several *ab-initio* calculations have already been performed to investigate the XMCD.^{25,26,28} The L_2 - and L_3 -edges involving electronic excitations of $2p$ -core electrons towards d -valence states have primarily attracted much attention due to dependence of the dichroic spectra on the exchange-splitting and the spin-orbit coupling of both initial core and final valence states. For $5d$ elements dissolved in $3d$ transition metals, the spin-orbit coupling of the initial $2p$ -core states is large and the resulting magnetic moment is small, while the opposite is true for the $3d$ elements. This can lead to a pronounced dichroic spectra as seen by Schültz in the case of $5d$ elements dissolved in iron.²³

In this work we study the correlation between the quantization axis dependent XMCD and the magnetic properties of both ordered alloys FePt and CoPt. Our method is based on an all-electron relativistic and spin-polarized full-potential muffin-tin orbital method (LMTO)^{29,30} in conjunction with both the von Barth and Hedin parameterization to the local density approximation (LSDA)³¹ and the generalized gradient approximation (GGA)³² to the exchange correlation potential. The implementation of the calculation of the XMCD spectra has been presented in a previous

work.²⁶ In section 2 we present the details of the calculations, while in sections 3 and 4 we discuss our MCA and the magnetic spin and orbital moments, respectively. In section 5 we present our calculated XMCD as a function of the spin quantization axis, and in section 6 we discuss the interpretation of the MCA using the band structure and the total density of states anisotropy.

II. COMPUTATIONAL DETAILS

To compute the electronic properties of CoPt and FePt we used the experimental lattice constants ($a=3.806\text{\AA}$ and $c/a=0.968$ for CoPt¹⁹; $a=3.861\text{\AA}$ and $c/a=0.981$ for FePt³⁴) and a unit cell containing one atom of cobalt(iron) and one of platinum. The $L1_0$ structure can be seen as a system of alternating cobalt(iron) and platinum layers along the [001] direction. The MCA and the XMCD are computed with respect to the angle γ between the [001] axis and the spin quantization axis on the (010) plane. So $\gamma=0^\circ$ corresponds to the [001] axis and $\gamma=90^\circ$ to the [100] axis.

MCA can be computed directly using *ab-initio* methods; it is defined as the difference between the total energy for two different spin quantization axis. The spin-orbit coupling contribution to MCA is implicitly included in our *ab-initio* calculations, and we do not take into account the many-body interactions of the spin-magnetic moments³⁵ since their contribution to the MCA is negligible.³⁶ The number of \mathbf{k} points for performing the Brillouin zone (BZ) integration depends strongly on the interplay between the contributions to the MCA from the Fermi surface and the remaining band structure contribution to the total energy.³⁷ When the former contribution to the MCA is important, a large number of \mathbf{k} -points is needed to describe accurately the Fermi surface. For the two studied systems we found that 6750 \mathbf{k} -points in the BZ are enough to converge the MCA within 0.1 meV.

To perform the integrals over the BZ we use a Gaussian broadening method which convolutes each discrete eigenvalue with a Gaussian function of width 0.1 eV. This method is known to lead to a fast and stable convergence of the spin and charge densities compared to the standard tetrahedron method. To develop the potential inside the MT spheres we calculated a basis set of lattice harmonics including functions up to $\ell = 8$, while for the FFT we used a real space grid of $16 \times 16 \times 20$. We used a double set of basis functions, one set to describe the valence states and one for the unoccupied states. For the valence electrons we used a basis set containing $3 \times s$, $3 \times p$ and $2 \times d$ wave functions, and for the unoccupied states $2 \times s$, $2 \times p$ and $2 \times d$ wave functions.

III. MAGNETO-CRYSTALLINE ANISOTROPY

CoPt and FePt films are known to present a strong uniaxial MCA, because of the high anisotropic $L1_0$ inter-metallic phase. Experimentally the magnetization axis is found to be along the [001] direction.^{38,39} In a first step we performed calculations with 250 \mathbf{k} -points in the BZ. This number of \mathbf{k} -points is large enough to produce accurate total energy when Gaussian smearing is used for the integration in the Brillouin Zone but not enough accurate to compute the MCA. In figure 1 we present calculations with respect to the angle γ between the [001] axis and the spin quantization axis on the (010) plane for the CoPt compound within the LSDA. We observe that total energy value increases with the angle γ . So the ground state corresponds to $\gamma=0^\circ$, *i.e.* the [001] axis. The same behavior occurs for the FePt compound. Because 250 \mathbf{k} -points are not enough to produce an accurate value for the MCA, we present in figure 2 the convergence of the MCA with the number of \mathbf{k} -points for both compounds within LSDA. The MCA is the difference in the total energy between the in-plane axis [100] and [110] and the easy axis [001]. We have found that the total energy difference between the [100] and the [110] directions is negligible compared to the difference between the in-plane axis and the [001] axis. Our values are converged up to 6750 \mathbf{k} -points and are given per unit cell (one atom of X and one of platinum). The MCA converges to 2.2 eV for CoPt and 3.9 eV for FePt. These behavior confirms the assumption that the system is isotropic inside the plane. The GGA MCA calculations converged to 1.9 meV and 4.1 meV for CoPt and FePt, respectively. The GGA results seem to be in good agreement with the LSDA results.

Daalderop *et al.*⁴⁰ performed calculations for MCA in CoPt and FePt by means of an LMTO method in the atomic sphere approximation (ASA) within LSDA³⁰ using the force theorem.⁴¹ The easy magnetization axis found by this latter calculation is the [001] for both systems in agreement with our LSDA and GGA results. Their MCA value is 2 meV for CoPt and is 3.5 meV for FePt. Solovyev *et al.*³⁷ used the same structure within a real-space Green's function technique framework to find also that the magnetization is along the [001] axis. Including the spin-orbit interaction for all the atoms, they found a CoPt MCA value of 2.3 meV and a FePt value of 3.4 meV. Our computed value agrees also with the value of 1.5 meV for CoPt and 2.8 meV for FePt, obtained by Sakuma⁴² using LMTO method in the atomic sphere approximation (ASA) in conjunction with the force theorem.⁴¹ The drawback of the LMTO-ASA method is that it accounts only for the spherical part of the potential and ignores the interstitial region. Furthermore, the force theorem does not account directly for the exchange-correlation contribution to the MCA. Finally, Oppeneer

used the augmented spherical waves method (ASW) in the atomic sphere approximation and found a MCA value of 2.8 meV for FePt and 1.0 meV for CoPt,⁴³ which are the smallest among all the *ab-initio* calculations.

Grange *et al.*,¹⁹ using a torque measurement for a MBE deposited CoPt film on a MgO(001) substrate, obtained a MAE of 1.0 meV. An early measurement of a monocrystal of CoPt, by Eurin and Pauleve, produced a value of 1.3 meV.³⁸ The large value of Eurin and Pauleve is due to the fact that their sample was completely ordered. For FePt the first experiment of Ivanov *et al.*⁴⁴ produced an anisotropy value of 1.2 meV and showed that for a thin film the shape anisotropy would be one order of magnitude smaller compared to the MCA. Farrow *et al.*³⁹ and Thiele *et al.*⁴⁵ found for MBE deposited FePt films on a MgO(001) substrate an anisotropy value of 1.8 meV. These films were highly ordered (more than 95% of the atoms were in the correct site). All experiments have been carried out at room temperature, which explain at some extent the difference between the calculated and experimental MCA values (the MCA decreases with temperature³⁸). It is worth mentioning that the experimental MCA for FePt is much larger than that of CoPt in agreement with our calculations. For thick films volume shape anisotropy (VSA) contributes also to the MAE and it favors always an in-plane magnetization axis. We can estimate the VSA as $-2\pi M_V^2$ in c.g.s. units, where M_V is the mean magnetization density,³⁶ and obtain a value of -0.1 meV for FePt and -0.06 meV for CoPt. These values are one order of magnitude smaller than the MCA values in agreement with the speculation of Ivanov *et al.*⁴⁴

IV. MAGNETIC MOMENTS

A. Density of States

In figure 3 we present the cobalt-projected partial density of states for three spin quantization axis corresponding to angles $\gamma = 0^\circ$, 45° and 90° calculated with 6750 \mathbf{k} -points. The 3- d states dominate the electronic structure of cobalt. The spin-up band is practically totally occupied while the spin down band is almost half-occupied. The general form of the cobalt DOS, as well as the iron DOS, does not seem to change appreciably with the angle γ . The platinum projected density of states show similar behavior for both FePt and CoPt compounds. Bulk platinum is paramagnetic and the small changes in the DOS come from the polarization of the 5 d electrons via hybridization with the 3 d electrons of cobalt (iron). It is worth mentioning that the DOS is calculated inside each muffin-tin and the interstitial region is not taken into account. To minimize the contribution of the interstitial region we use almost touching muffin-tin spheres. In addition, we have find that remaining region has a negligible spin polarization.

B. Spin Magnetic Moments

The spin magnetic moments are isotropic with respect to the spin quantization axis as expected. They were calculated by attributing all the charge inside each muffin-tin sphere to the atom located in that sphere. As outlined above we have found that the interstitial contribution to the spin magnetic moment is one order of magnitude smaller than that of the platinum site. In CoPt we found a cobalt spin magnetic moment of $1.79 \mu_B$ and a platinum moment of $0.36 \mu_B$ within the LSDA. The GGA cobalt spin magnetic moment of $1.83 \mu_B$ is slightly larger than the value within LSDA. This is due to a more atomic like description of the atoms in a solid within the GGA compared to the LSDA. Although the GGA underestimates the hybridization between cobalt and platinum d valence electrons compared to the LSDA, the larger cobalt spin moment leads to a slightly larger GGA platinum spin moment of $0.37 \mu_B$. Our calculated values are in good agreement with the experimental values of Grange *et al.* ($1.75 \mu_B$ for cobalt and $0.35 \mu_B$ for platinum).¹⁹ Previous experiments by van Laar on a powder sample gave a value of $1.7 \mu_B$ for the cobalt atom and 0.25 for the platinum atom.⁴⁶ The spin magnetic moments have been previously calculated by Solovyev *et al.*³⁷ (1.72 for cobalt and 0.37 for platinum), by Daalderop *et al.*⁴⁰ (1.86 for cobalt), by Sakuma⁴² (1.91 for cobalt and 0.38 for platinum), and finally by Kootte *et al.*⁴⁷ by means of a localized spherical wave method (1.69 for cobalt and 0.37 for platinum). All previous calculations are in good agreement with our full-potential results.

As expected the iron spin moments are much larger than the cobalt ones. The LSDA produced a value of $2.87 \mu_B$ while the GGA produced a slightly larger value, $2.96 \mu_B$. The hybridization between the iron 3 d states and the platinum 5 d states is less intense than in the case of CoPt resulting in a smaller platinum moment for FePt. The LSDA platinum spin moment is $0.33 \mu_B$ (compared to $0.36 \mu_B$ in CoPt) and the GGA platinum spin moment is $0.34 \mu_B$ (compared to $0.37 \mu_B$ in CoPt). The spin magnetic moments have been previously calculated by Solovyev *et al.*³⁷ (2.77 for iron and 0.35 for platinum), by Daalderop *et al.*⁴⁰ (2.91 for iron), by Sakuma⁴² (2.93 for iron and 0.33 for platinum), and finally by Osterloch *et al.*⁴⁸ (2.92 for iron and 0.38 for platinum). Here again all previous calculations

are in good agreement with our full-potential results. All the methods produced a smaller induced spin moment for platinum atom in FePt than for CoPt, verifying that the hybridization effect in CoPt is much stronger than in FePt.

C. Orbital Magnetic Moments

Contrary to spin moments, the orbital moments are anisotropic. Figure 4 presents the behavior of the orbital moments as a function of the angle γ between the [001] direction and the spin quantization axis within LSDA for both CoPt and FePt compounds (the lines are guide to the eye). The orbital moments decrease with respect to the angle γ but the values for the [100] axis does not follow this general trend. All four lines seem to have the same behavior, but it is interesting to notice that for the CoPt and magnetization along the [100] axis cobalt orbital moment is smaller than the platinum one (for the values see Tables I and II). The cobalt moments decrease faster than platinum moments in CoPt. For the iron and platinum atoms in FePt the two lines are practically parallel. The platinum orbital moments in FePt are smaller than for the CoPt with a factor that varies from 73% for $\gamma=0^\circ$ to 67% for $\gamma=90^\circ$. The ratio of iron and platinum orbital moments in FePt varies from 1.56 for $\gamma=0^\circ$ down to 1.35 for $\gamma=90^\circ$, which is considerably smaller than the ratio of cobalt and platinum orbital moments in CoPt. We notice here that in our calculations we can estimate only the projection of the total orbital moment on the spin quantization axis and we have no information concerning the real value of the total magnetic moment or its direction in space. It seems that for the magnetization along the [100] direction, the direction of the orbital magnetic moment undergoes a discontinuous jump, resulting in a large projection on the spin quantization axis with respect to γ at the vicinity of 90° . This behavior is also reproduced by the GGA.

In Table I we present the values of the orbital moments of iron and cobalt within both the LSDA and GGA as a function of the angle γ . The GGA values seem to be smaller than the LSDA ones but follow exactly the same trends. The orbital moment anisotropy is more important in the case of cobalt. The LSDA cobalt orbital moment changes by $0.048 \mu_B$ and the GGA moment by $0.027 \mu_B$ as we pass from the easy axis [001] to the hard axis [100]. The LSDA iron moment changes by $0.002 \mu_B$ and the GGA moment is the same for the two high symmetry directions. In the case of cobalt the difference between values calculated within the two functionals, LSDA and GGA, becomes smaller when the angle increases and for 75° it changes sign. In the case of iron this difference decreases only slightly with the angle but since the difference is considerably smaller than in CoPt (less than 0.004), we conclude that the orbital moment in the LSDA and the GGA are roughly the same.

In Table II we present the values for the platinum orbital moment within both functionals. We see that the GGA produces larger moments than the LSDA for platinum in FePt contrary to CoPt. The platinum moments are in general smaller than the moments of the $3d$ ferromagnets, and the difference between the values calculated within LSDA and GGA are small. The absolute values for platinum are comparable to cobalt(iron) orbital moments even though the spin moments on platinum are one order of magnitude smaller than for cobalt(iron). The large orbital moments for platinum are due to a much larger spin-orbit coupling for the d electrons of the platinum compared to the $3d$ ferromagnets.

The orbital moments of FePt and CoPt have been previously calculated by Daalderop and collaborators⁴⁰ and by Solovyev and collaborators³⁷ for the [001] direction using the LSDA. The orbital moment of the cobalt site was found to be $0.12 \mu_B$ by Daalderop and $0.09 \mu_B$ by Solovyev. The value of Daalderop is closer to our LSDA value of $0.11 \mu_B$. For iron site Daalderop found a value of $0.08 \mu_B$ and Solovyev $0.07 \mu_B$ in good agreement with our LSDA value. The platinum orbital moment has been calculated by Solovyev. He found a value of $0.06 \mu_B$ for platinum in CoPt and $0.044 \mu_B$ for platinum in FePt, close to our values, $0.06 \mu_B$ and $0.05 \mu_B$, respectively.

On the other hand, experimental data are available for CoPt by Grange;¹⁹ obtained by applying the sum rules to the experimental XMCD spectra. The sum rules give the moments per hole in the d -band. To compare experiment with theory we calculated the number of d -holes by integrating the d projected density of states inside each muffin-tin sphere. We found 2.63 d and 2.48 d holes for cobalt and platinum, respectively. The cobalt orbital moment varies from $0.26 \mu_B$ for $\gamma=10^\circ$ down to $0.11 \mu_B$ for $\gamma=60^\circ$. The measured values are also available for two other angles: $0.24 \mu_B$ for $\gamma=30^\circ$ and $0.17 \mu_B$ for $\gamma=45^\circ$. Our theory reproduces qualitatively the experimental trends but underestimates the absolute values by more than 50% (see Tables I and II for all the values). The calculated values show a less sharp decrease with the angle than the experimental ones. For platinum the experimental data are available only for two angles 10° and 60° . For $\gamma=10^\circ$ the orbital moment is $0.09 \mu_B$ and for $\gamma=60^\circ$ it is $0.06 \mu_B$. For the platinum site the calculated values are in much better agreement than for the cobalt site but we must keep in mind that the sum rules have their origin in an atomic theory and their use for $5d$ itinerant electrons like in platinum is still debated. The discrepancy between the theory and the experiment comes mainly from the approximation to the exchange and correlation. Both the LSDA and the GGA approximations to the density functional theory are known to underestimate the orbital moment values, because the orbital moment is a property directly associated with the current in the solid

and a static image is not sufficient. But until now a DFT formalism like the current and spin density functional theory (CS-DFT),⁴⁹ which can treat at the same footing the Kohn-Sham and the Maxwell equations is too heavy to implement in a full-potential *ab-initio method*. The other problem is that there is no form of the exchange energy of a homogeneous electronic gas in a magnetic field known and this is the main quantity entering the CS-DFT formalism. Brooks has also developed an *ad hoc* correction to the Hamiltonian to account for the orbital polarization but this correction originates from an atomic theory and its application to itinerant systems is not satisfactory.⁵⁰

V. XMCD

XMCD spectroscopy became popular after the development of the sum rules that enable the extraction of reliable information on the micro-magnetism directly from the experimental spectra.^{14,15} The great advantage of XMCD is that we can probe each atom and orbital in the system so to obtain information on the local magnetic properties. Lately angle-dependent XMCD experiments allowed the determination of magnetic properties for different spin quantization axis. All experimental spectra for CoPt have been obtained by Grange *et al*,¹⁹ and all calculated spectra presented in this section were obtained using the LSDA. The GGA produced the same results and are not presented.

Figure 5 presents the XMCD spectra for cobalt and iron atoms for the [100] and [001] magnetization axis. We convoluted our theoretical spectra using a Lorentzian width of 0.9 eV and a Gaussian width of 0.4 eV as proposed by Ebert,²⁵ in the case of iron to account for the core hole effect and the experimental resolution, respectively. The energy difference between the L_3 and L_2 peaks is given by the spin-orbit splitting of the $p_{\frac{1}{2}}$ and $p_{\frac{3}{2}}$ core states. It is larger in the case of cobalt, 14.8 eV, than for iron, 12.5 eV. The intensities of the peaks are comparable for both atoms, but the cobalt peak-intensities are larger for the [001] axis contrary to the iron spectrum. The most important feature of these spectra is the integrated L_3/L_2 branching ratio as it enters the sum rules. It is larger in the case of cobalt site. This is expected since the sum rules predict that a larger L_3/L_2 ratio is equivalent to a larger orbital moment. For both atoms the integrated L_3/L_2 branching ratio is larger for the [001] axis. But the ratio anisotropy is larger for the cobalt site (1.32 for $\mathbf{M}||[001]$ and 1.17 for $\mathbf{M}||[100]$) than for the iron site (1.15 for $\mathbf{M}||[001]$ and 1.14 for $\mathbf{M}||[100]$) reflecting the larger orbital moment anisotropy of cobalt compared to iron (see Table I). Especially for iron both orbital moment and integrated L_3/L_2 branching ratio are practically the same for both magnetization axis. As these changes in the XMCD signal are related to the change in the orbital magnetic moment between the two magnetization directions. The XMCD anisotropy should be roughly proportional to the underlying MCA but no relation exist that connects these two anisotropies. However they are connected indirectly through the orbital moment anisotropy.⁵¹

In figure 6 we have plotted the platinum XMCD spectra for two angles $\gamma=10^\circ$ and 60° for both compounds. The life time of the core-hole in platinum is smaller than for cobalt so the broadening used to account for its life time should be larger. We used both a Lorentzian (1 eV) and a Gaussian (1 eV) to represent this life time and a Gaussian of 1 eV width for the experimental resolution. As in the case of cobalt and iron the platinum XMCD spectra change with the angle and depend on the surrounding neighbors. The peak intensities are larger in CoPt. Also the difference in the intensity due to the anisotropy has different sign in the two compounds. The intensities of FePt spectra for $\gamma=10^\circ$ are much larger than for $\gamma=60^\circ$ contrary to the CoPt behavior. As is the case for cobalt in CoPt, the platinum site integrated L_3/L_2 branching ratio shows larger anisotropy than for platinum in FePt. In CoPt it is 1.49 for $\gamma=10^\circ$ and 1.19 for $\gamma=60^\circ$, while for FePt it is 1.20 for $\gamma=10^\circ$ and 1.14 for $\gamma=60^\circ$. Here again the XMCD follows the anisotropy of the orbital magnetic moment in these compounds. The energy difference between the two peaks is 1727 eV for both compounds. The $2p$ electrons of platinum are deep in energy and are little influenced by the local environment, so that their spin-orbit splitting does not depend on the neighboring atoms of platinum.

We expect a better agreement between the theoretical and the experimental XMCD spectra for the platinum site than for the cobalt site, because the core hole is deeper and would effect less the final states of the photo-excited electron. In figure 7, we have plotted the absorption and the XMCD spectra of cobalt for $\gamma=0^\circ$. We have scaled our spectra in a way that the experimental and theoretical L_3 peaks in the absorption spectra have the same intensity. The energy difference between the L_3 and L_2 peaks is in good agreement with experiment. But the intensity of the L_2 peak is larger than the corresponding experimental peak. The high intensity of the calculated L_2 edge makes the theoretical XMCD integrated L_3/L_2 branching ratio of 1.32 much smaller than the experimental ratio of 1.72. This is because the LSDA fails to represent the physics of the core hole photo-excited electron recombination. In the case of $3d$ ferromagnets the core hole is shallow and influences the final states seen by the photo-excited electron. A formalism that can treat this electron-hole interaction has been proposed by Schwitalla and Ebert,⁵² but it failed to improve the L_3/L_2 branching ratio of XAS of the late transition metals. Benedict and Shirley⁵³ have also developed a scheme to treat this phenomena but its application is limited only to crystalline insulators.

In figure 8 we have plotted experimental and theoretical total absorptions for the platinum atom in CoPt. For

both L_2 and L_3 edges the theory gives a sharp peak which does not exist in experiment. As expected the L_3 peak is much more intense than the L_2 . In contrast to what is obtained for cobalt, the results for the platinum XMCD (see figure 9) show better agreement with experiment, due to the fact that the core hole effect is less intense (core hole much deeper compared to cobalt). The experimental and theoretical L_2 and L_3 edges are separated by a spin-orbit splitting of the $2p$ core states of 1709 and 1727eV respectively. The width of both L_2 and L_3 edges is comparable to experiment, but the calculated L_2 edge is much larger. This produces a calculated integrated branching ratio of 1.49 which is much smaller than the experimental ratio of 2.66. Here again the theory is underestimating the branching ratio.

VI. BAND STRUCTURE AND DENSITY OF STATES ANISOTROPY

In figure 10 we present the band structure along the [001] and [100] axis in the reciprocal space for different angles γ for the CoPt compound within the LSDA. We know that it is essentially the area around the Fermi level that changes with respect to the spin quantization axis. For this reason we have enlarged a region of ± 1 eV around the Fermi level. In the first panel we plot the relativistic band structure for $\gamma=0^\circ$. In the second and third panel we have plotted the relativistic band structure for $\gamma=45^\circ$ and $\gamma=90^\circ$. We remark that as the angle increases there are bands that approach the Fermi level and cross it. However this information concerns just two high symmetry directions. For this reason we limited ourselves to the changes in the total DOS. In figure 11 we notice that just below the Fermi level the DOS for the hard axis is lower than for the easy axis which seems to favor the hard axis. This means that the anisotropy does not originate from the changes at the vicinity of the Fermi level but from that of the whole DOS. It is difficult to investigate this phenomena by inspection of the changes at the vicinity of the Fermi surface and to explain the sign of the MCA. Our results confirm the work of Daalderop and collaborators⁵⁴ that argued that not only states in the vicinity of the Fermi surface contribute to the MAE, as originally thought,⁵⁵ but states far away make an equally important contribution.

VII. CONCLUSION

We have performed a theoretical *ab-initio* study of the magnetic properties of the ordered CoPt and FePt fct alloys systems. The calculated easy axis is the [001] for both compounds in agreement with other calculations and with experiments on films which found a strong perpendicular magnetization axis. The density of states is found to change very little with the direction of the spin quantization axis, and hence the magnetic moments are isotropic with respect to the magnetization axis. Contrary to the spin moments, the orbital magnetic moments decrease with the angle γ up to 75° (γ is the angle between the spin quantization axis and the [001] axis).

The calculated x-ray magnetic circular dichroism (XMCD) for all the atoms reflect the behavior of the orbital moments. Especially platinum resolved spectra present large differences between the two compounds. Cobalt XMCD spectra are in agreement with experiment but as usual the L_3/L_2 ratio is underestimated by the theory. The platinum site shows better agreement with experiments because the core-hole is much deeper than in the case of cobalt.

Finally we showed that all the occupied electronic states contribute to the magneto-crystalline anisotropy and not just states near the Fermi level for both CoPt and FePt.

ACKNOWLEDGMENTS

We thank J. M. Wills for providing us with his FPLMTO code. I.G. is supported by an European Union grant N° ERBFMXCT96-0089. The calculations were performed using the SGI Origin-2000 supercomputer of the Université Louis Pasteur de Strasbourg and the IBM SP2 supercomputer of the CINES under grant gem1917.

¹ S. S. A. Razee, J. B. Staunton, and F. J. Pinski, Phys. Rev. B **56**, 8082 (1996); S. S. A. Razee, J. B. Staunton, F. J. Pinski, B. Ginatempo, and E. Bruno J. Appl. Phys. **83**, 7097 (1998).

² S. S. A. Razee, J. B. Staunton, B. Ginatempo, F. J. Pinski, and E. Bruno, Phys. Rev. Lett. **82**, 5369 (1999).

- ³ K. R. Coffey, M. A. Parker, and J. K. Howard, *IEEE Trans. Magn.* **31**, 2737 (1995); S. H. Charap, P. -L. Lu, and Y. He, *IEEE Trans. Magn.* **33**, 978 (1997); N. Li and B. M. Lairson, *IEEE Trans. Magn.* **35**, 1077 (1999).
- ⁴ G. R. Harp, D. Weller, T. A. Rabedeau, R. F. C. Farrow, and R. F. Marks, *Mat. Res. Soc. Symp. Proc.* **313**, 493 (1993).
- ⁵ A. Cebollada, D. Weller, J. Sticht, G. R. Harp, R. F. C. Farrow, R. F. Marks, R. Savoy, and J. C. Scott, *Phys. Rev. B* **50**, 3419 (1994).
- ⁶ M. R. Visokay and R. Sinclair, *Appl. Phys. Letters* **66**, 1692 (1995).
- ⁷ C. -J. Lin and G. L. Gorman, *Appl. Phys. Lett.* **61**, 1600 (1992).
- ⁸ M. Watanabe and M. Homma, *Jpn. J. Appl. Phys.* **35**, L1264 (1996).
- ⁹ B. M. Lairson, M. R. Visokay, R. Sinclair, and B. M. Clemens, *Appl. Phys. Lett.* **62**, 639 (1993).
- ¹⁰ M. Watanabe, K. Takanashi, and . Fujimori, *J. Magn. Magn. Mat.* **113**, 110 (1991).
- ¹¹ S. Mitani, K. Takanashi, M. Sano, H. Fujimori, A. Osawa, and H. Nakajima, *J. Magn. Magn. Mat.* **148**, 163 (1995).
- ¹² K. Sato, H. Hongu, H. Ikekame, Y. Tosaka, M. Watanabe, K. Takanashi, and H. Fujimori, *Jpn. J. Appl. Phys.* **32**, 989 (1993).
- ¹³ D. Weller, J. Stöhr, R. Nakajima, A. Carl, M. G. Samant, C. Chappert, R. Mégy, P. Beauvillain, P. Veillet, and G. A. Held, *Phys. Rev. Lett.* **75**, 3752 (1995).
- ¹⁴ B. T. Thole, P. Carra, F. Sette, and G. van der Laan, *Phys. Rev. Lett.* **68**, 1943 (1992).
- ¹⁵ P. Carra, B. T. Thole, M. Altarelli, and X. Wang, *Phys. Rev. B* **70**, 694 (1993).
- ¹⁶ G. van der Laan, *Phys. Rev. B* **57**, 112 (1998).
- ¹⁷ C. T. Chen, Y. U. Idzerda, H.- J. Lin, N. V. Smith , G. Meigs, E. Chaban, G. H. Ho, E. Pellegrin, and F. Sette, *Phys. Rev. Lett.* **75**, 152 (1995).
- ¹⁸ R. Wu, D. Wang, and A. J. Freeman, *Phys. Rev. Lett.* **71**, 3581 (1993); R. Wu and A. J. Freeman, *ibid* **73**, 1994 (1994).
- ¹⁹ W. Grange, thesis, Université Louis Pasteur, Strasbourg, 1998.
- ²⁰ N. Nakajima, T. Koide, T. Shidara, H. Miyauchi, H. Fukutani, A. Fujimori, K. Iio , T. Katayama, M. Nývlt, and Y. Suzuki, *Phys. Rev. Lett.* **81**, 5229 (1998).
- ²¹ T. Koide, N. Nakajima, T. Shidara, H. Miyauchi, H. Kawabe, H. Fukutani, A. Fujimori, K. Iio, T. Katayama, and Y. Suzuki, *J. Appl. Phys.* **79**, 5708 (1996).
- ²² S. Rüegg, G. Schütz, P. Fischer, R. Wienke, W. P. Zeper, and H. Ebert, *J. Appl. Phys.* **69**, 5655 (1991).
- ²³ G. Schültz *et al.*, *Z. Phys. B* **75**, 495 (1989).
- ²⁴ E. K. Hlil, R. Baudouin-Savois, B. Moraweck, and A. J. Renouprez, *J. Phys. Chem.* **100**, 3102 (1996).
- ²⁵ H. Ebert, *Rep. Prog. Phys.* **59**, 1665 (1996).
- ²⁶ M. Alouani, J. M. Wills, and J. W. Wilkins, *Phys. Rev. B* **57**, 9502 (1998).
- ²⁷ I. Galanakis, S. Ostanin, M. Alouani, H. Dreyssé, and J. M. Wills, *Phys. Rev. B* **61**, 599 (2000).
- ²⁸ C. Brouder and M. Hikam, *Phys. Rev. B* **43**, 3809 (1991); C. Brouder, M. Alouani, and K. H. Bennamann, *Phys. Rev. B* **54**, 7334 (1996); G. Y. Guo, *Phys. Rev. B* **57**, 10 295 (1998); A. Ankudinov and J. J. Rehr, *Phys. Rev. B* **56**, 1712 (1997); A. Ankudinov, B. Ravel, J. J. Rehr, and S. Conradson, *Phys. Rev. B* **58**, 7565 (1998); G. van der Laan and B. T. Thole, *Phys. Rev. B* **43**, 13 401 (1991).
- ²⁹ J. M. Wills and B. R. Cooper, *Phys. Rev. B* **36**, 3809 (1987); M. Alouani and J. M. Wills, *Phys. Rev. B* **54**, 2480 (1996).
- ³⁰ O. K. Andersen, *Phys. Rev. B* **12**, 3060 (1975).
- ³¹ U. von Barth and L. Hedin, *J. Phys. C: Solid State Phys.* **5**, 1629 (1972).
- ³² J. P. Perdew and Y. Wang, *Phys. Rev. B* **33**, 8800 (1986); *ibid.* **45**, 13244 (1992).
- ³³ P. Hohenberg and W. Kohn, *Phys. Rev. B* **136**, 864 (1964); W. Kohn and L. J. Sham, *Phys. Rev. A* **140**, 1133 (1965).
- ³⁴ P. Villars and L. D. Calvet: *Pearson's Handbook of Crystallographic Data for Intermetallic Phases*, (Metals Park, OH: American Society for Metals, 1985).
- ³⁵ H. J. F. Jansen, *Phys. Rev. B* **38**, 8022 (1988).
- ³⁶ P. Bruno, *Physical Origins and Theoretical Models of Magnetic Anisotropy*, Ferienkurse des Forschungszentrum Jülich, Jülich (1993).
- ³⁷ I. V. Solovyev, P. H. Dederichs, and I. Mertig, *Phys. Rev. B* **52**, 13 419 (1995).
- ³⁸ P. Eurin and J. Pauleve, *IEEE Trans. Mag.* **5**, 216 (1969).
- ³⁹ R. F. C. Farrow, D. Weller, R. F. Marks, M. F. Toney, A. Cebollada, and G. R. Harp, *J. Appl. Phys.* **79**, 5967 (1996).
- ⁴⁰ G. H. O. Daalderop, P. J. Kelly, and M. F. H. Shuurmans, *Phys. Rev. B* **44**, 12 054 (1991).
- ⁴¹ A. R. Macintosh and O. K. Andersen, *Electrons at the Fermi Surface* (Cambridge/Cambridge Univ. Press, 1980).
- ⁴² A. Sakuma, *J. Phys. Soc. Jap.* **63**, 3053 (1994).
- ⁴³ P. Oppeneer, *J. Magn. Magn. Mat.* **188**, 275 (1998).
- ⁴⁴ O. A. Ivanov, L. V. Solina, V. A. Demshina, and L. M. Magat, *Fiz. Metal. Metaloved.* **35**, 92 (1973).
- ⁴⁵ J. -U. Thiele, L. Folks, M. F. Toney, and D. K. Weller, *J. Appl. Phys.* **84**, 5686 (1998).
- ⁴⁶ B. van Laar, *J. Physique* **25**, 600 (1964).
- ⁴⁷ A. Kootte, C. Haas, and R. A. de Groot, *J. Phys.: Cond. Matt.* **3**, 1133 (1991).
- ⁴⁸ I. Osterloch, P. M. Oppeneer, J. Sticht and J. Kübler, *J. Phys.: Condens. Matter* **6**, 285 (1994).
- ⁴⁹ G. Vignale and M. Resolt, *Phys. Rev. B* **37**, 10 685 (1998).
- ⁵⁰ M. S. S. Brooks, *Physica B* **130**, 6 (1985).

⁵¹ P. Bruno, Phys. Rev. B **39**, 865 (1989); G. van der Laan, J. Phys. Cond. Matt. **10**, 3239 (1998).

⁵² J. Schwitalla and H. Ebert, Phys. Rev. Lett. **80**, 4586 (1998).

⁵³ L X. Benedict and E. L. Shirley, Phys. Rev. B **59**, 5441 (1999).

⁵⁴ G. H. O. Daalderop, P. J. Kelly, and M. F. H. Schuurmand, Phys. Rev. Lett. **71**, 2165 (1993).

⁵⁵ D. S. Wang, R. Wu, and A. J. Freeman, Phys. Rev. Lett. **70**, 869 (1993); D. S. Wang, R. Wu, and A. J. Freeman, Phys. Rev. Lett. **71**, 2166 (1993).

TABLE I. Calculated LSDA and GGA cobalt(iron) orbital magnetic moments with respect to the angle γ between the [001] axis and the spin quantization axis in the (010) plane. For both atoms the orbital moments decrease with the angle but values for $\gamma=90^\circ$ do not follow this trend. Both LSDA and GGA produce the same trends. The moments at the cobalt site are larger than at the iron site. The experimental orbital moments for the cobalt site are taken from the Ref. 19. The theory underestimates the experimental orbital moments by more than 50% but reproduces the correct trends.

γ	0°	10°	30°	45°	60°	75°	90°
Fe-LSDA	0.072	0.070	0.062	0.051	0.036	0.019	0.070
Fe-GGA	0.068	0.067	0.059	0.048	0.034	0.018	0.068
Co-LSDA	0.109	0.107	0.095	0.076	0.052	0.022	0.061
Co-GGA	0.088	0.087	0.077	0.063	0.044	0.023	0.061
Co-Exp		0.26	0.24	0.17	0.11		

TABLE II. Calculated LSDA and GGA orbital moments of platinum in FePt and CoPt with respect to the angle γ between the [001] axis and the spin quantization axis in the (010) plane. For the FePt the GGA produces larger values than LSDA contrary to CoPt. The moments decrease with the angle but increase sharply at $\gamma=90^\circ$. The moments are significantly larger for the CoPt compound. Experimental results for platinum in CoPt are taken from the Ref. 19. The agreement is better than in the case of cobalt.

γ	0°	10°	30°	45°	60°	75°	90°
FePt-LSDA	0.046	0.045	0.039	0.032	0.023	0.012	0.052
FePt-GGA	0.049	0.048	0.043	0.035	0.025	0.013	0.058
CoPt-LSDA	0.063	0.061	0.054	0.044	0.030	0.014	0.078
CoPt-GGA	0.061	0.060	0.053	0.043	0.031	0.016	0.072
CoPt-Exp		0.09			0.06		

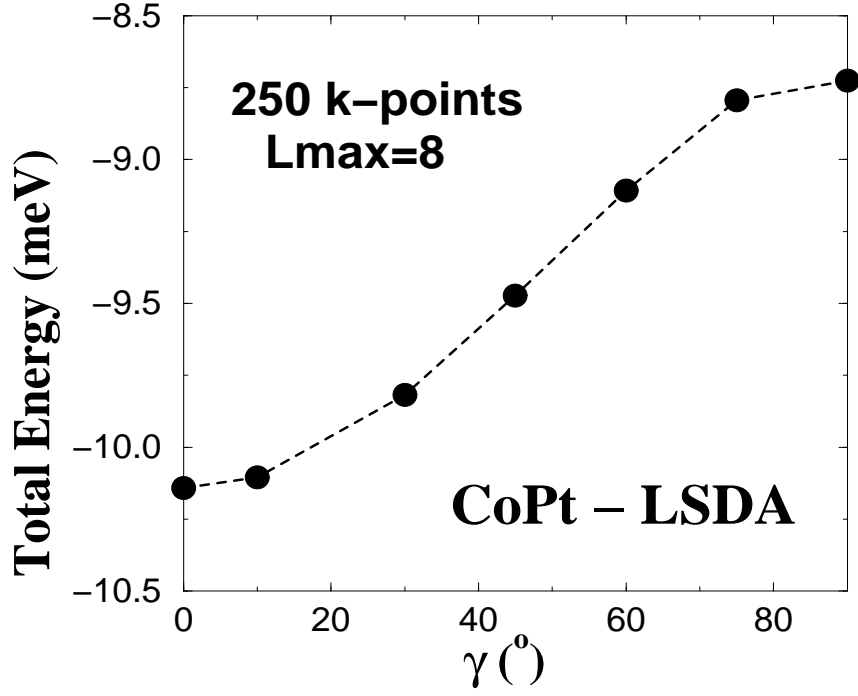


FIG. 1. Total energy for the CoPt system within LSDA as a function of the angle γ between the [001] axis and the spin quantization axis on the (010) plane. The fundamental state corresponds to $\gamma=0^\circ$, that means to the [001] axis. The total energy increases as a function of γ .

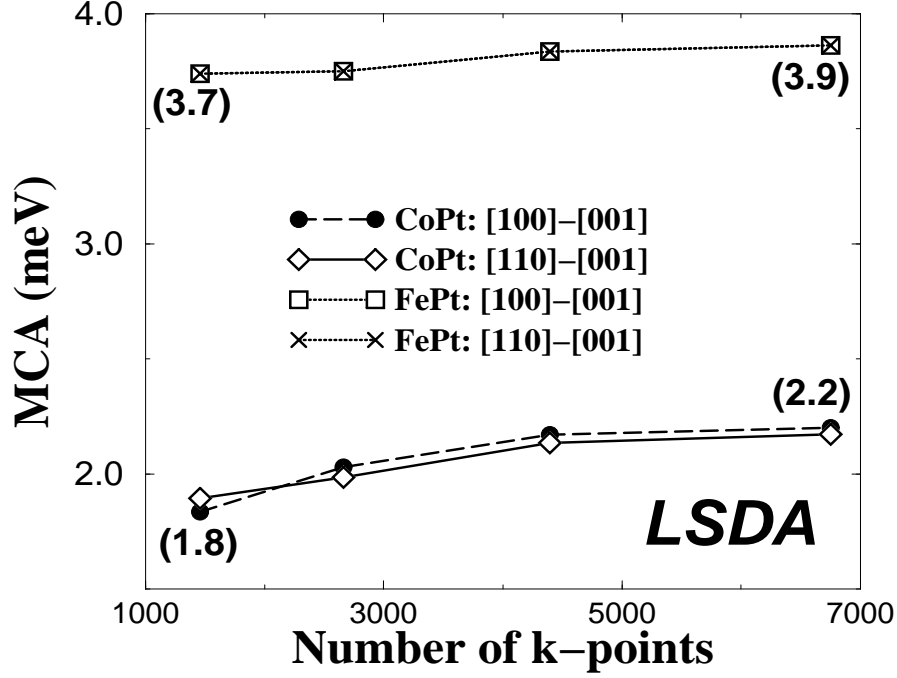


FIG. 2. Convergence of the magneto crystalline anisotropy in meV with respect to the number of k -points. The calculation is performed for two in-plane axis. For CoPt the line for the $[100]$ axis converges to 2.2 meV while the line for the $[110]$ axis converges to 2.17 meV. For FePt the two lines differ by less than 0.01 meV. The behavior of MCA verifies the assumption that the $L1_0$ structure is isotropic in the (001) plane.

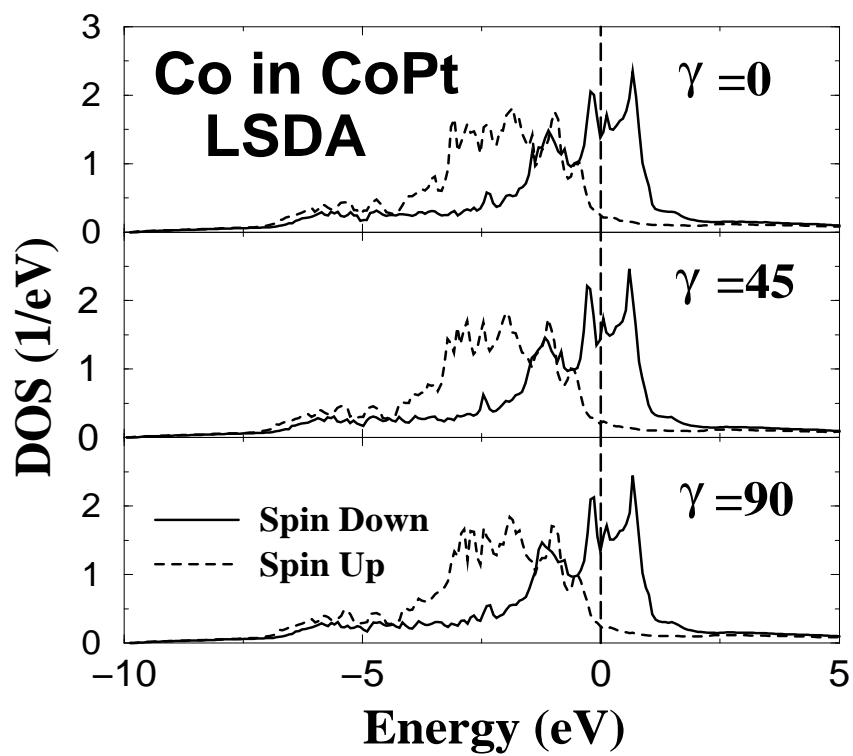


FIG. 3. Cobalt projected partial density of states with respect to the angle γ between the $[001]$ axis and the spin quantization axis in the (010) plane. There are no major changes with γ . This behavior reflect the isotropic character of the spin moments.

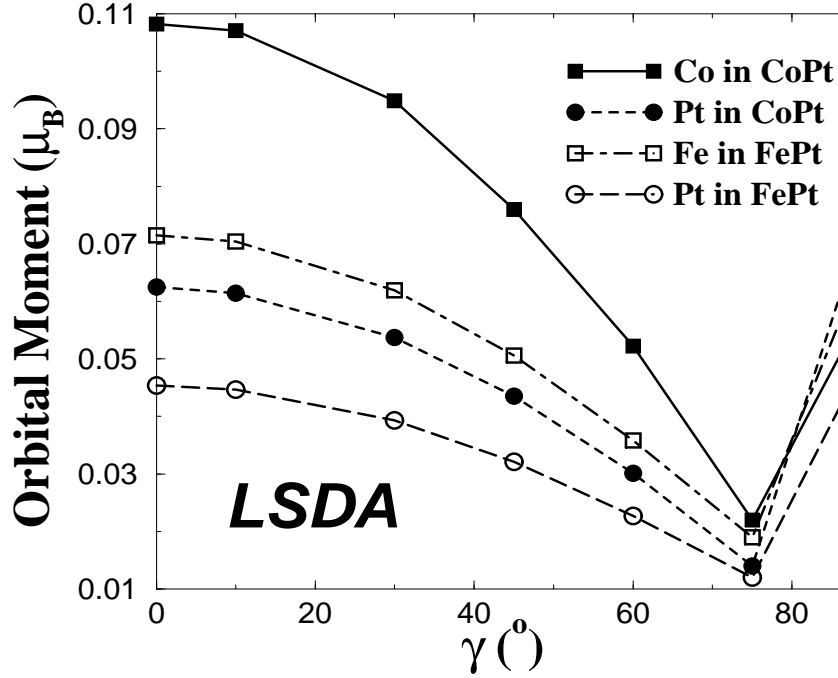


FIG. 4. Calculated orbital moments for both compounds within LSDA as a function of the angle γ between the [001] direction and the spin quantization axis (the lines are guides for the eye). All four atoms show the same behavior. The orbital moments decrease with the angle γ until about 75° , then they increase. The moments for the CoPt compound are larger than for these of FePt.

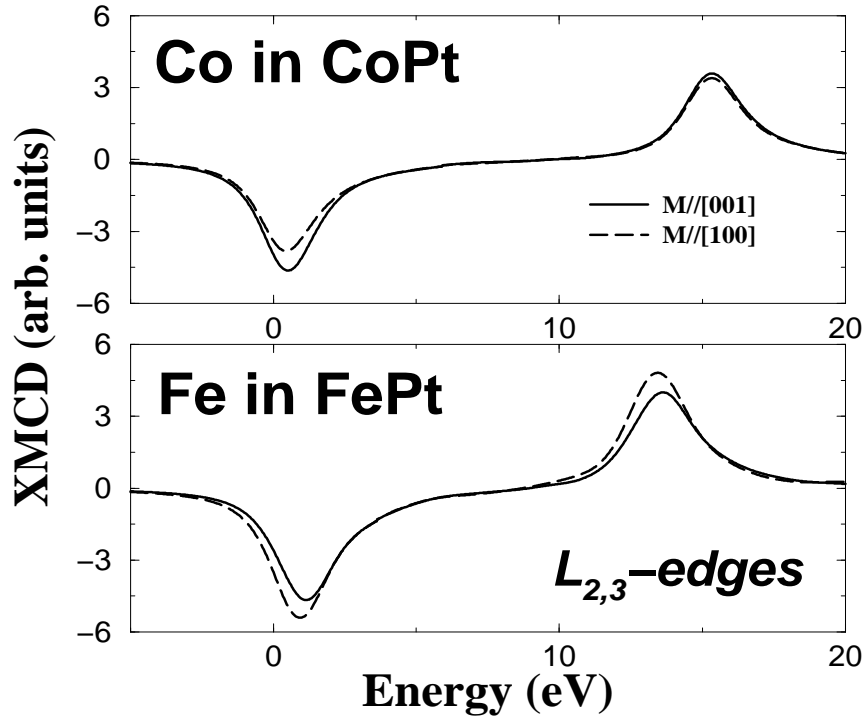


FIG. 5. XMCD spectra for the cobalt and iron sites in the two XPt compounds and for magnetization along the two high symmetry axis ($[001]$ and $[100]$). The iron and cobalt XMCD show different behavior. The peaks intensities for the cobalt spectrum lay higher for $M\parallel[001]$ and the L_3/L_2 integrated branching ratio is larger for this axis. Contrary, the peaks intensity for the iron site are larger for $M\parallel[100]$ and the L_3/L_2 integrated branching ratio is about constant.

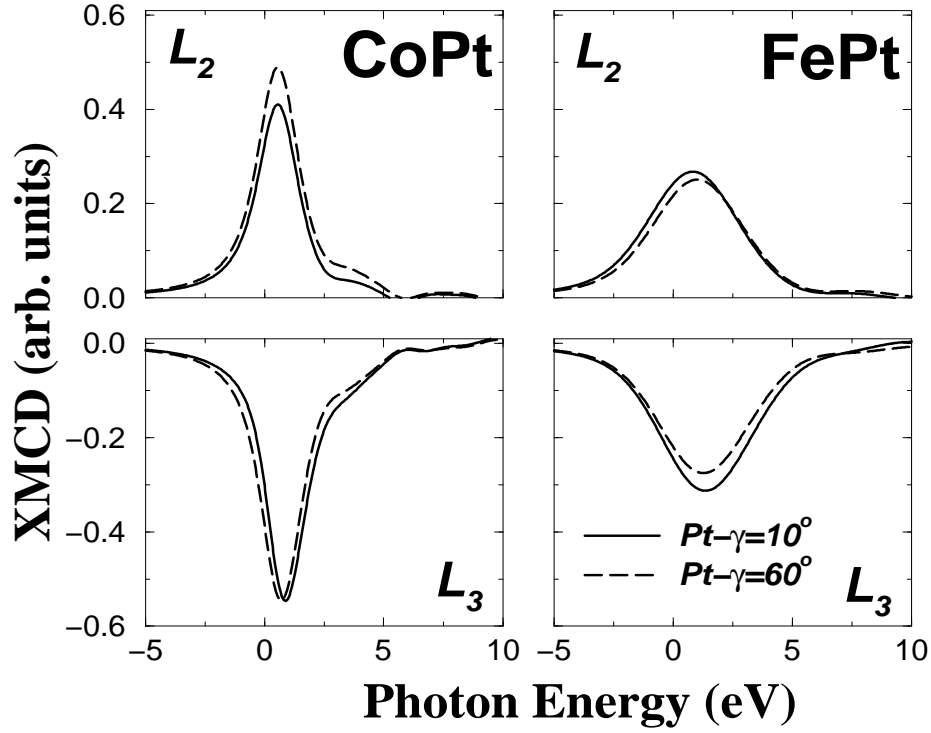


FIG. 6. XMCD spectra for platinum for two values of the angle γ between the [001] direction and the spin quantization axis in both compounds. The differences in the XMCD are important and the L_3/L_2 integrated branching ratio changes considerably with the angle. The intensities for the CoPt compound are larger reflecting the bigger orbital moments in this compound. The spin-orbit splitting of the core $p_{\frac{1}{2}}$ and $p_{\frac{3}{2}}$ states is 1727eV in both compounds.

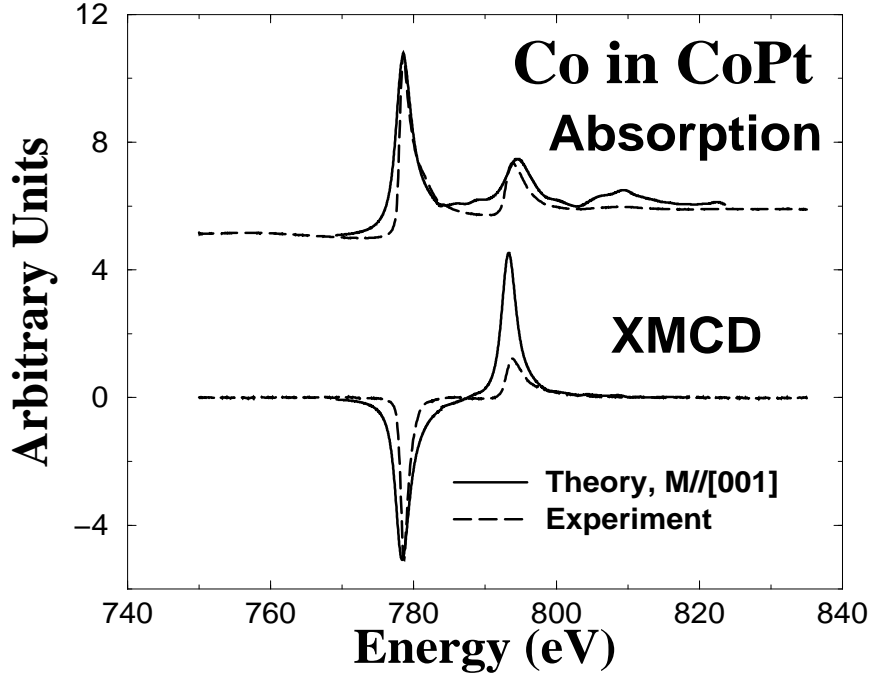


FIG. 7. Theoretical and experimental absorption and XMCD spectra for the cobalt site in CoPt for $\gamma=0^\circ$, where γ the angle between the [001] direction and the spin quantization axis. The theory overestimates the absorption at the L_2 edge and underestimates the L_3/L_2 integrated branching ratio.

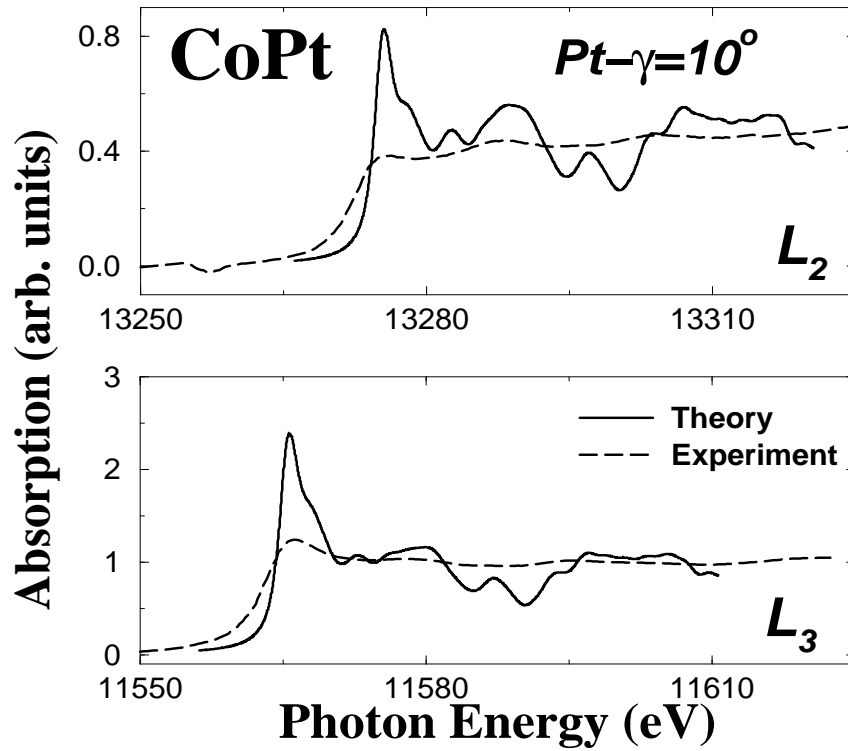


FIG. 8. Calculated and experimental absorption spectra at the platinum site and for $\gamma=10^\circ$ in CoPt, where γ is the angle between the [001] direction and the spin quantization axis. The theory produces a peak at the threshold of both $L_{2,3}$ edges. Both experimental and theoretical spectra have the same shape for the two edges but L_3 edge is much more intense. Most of the structures in the experimental spectra are washed out due to a strong broadening effect.

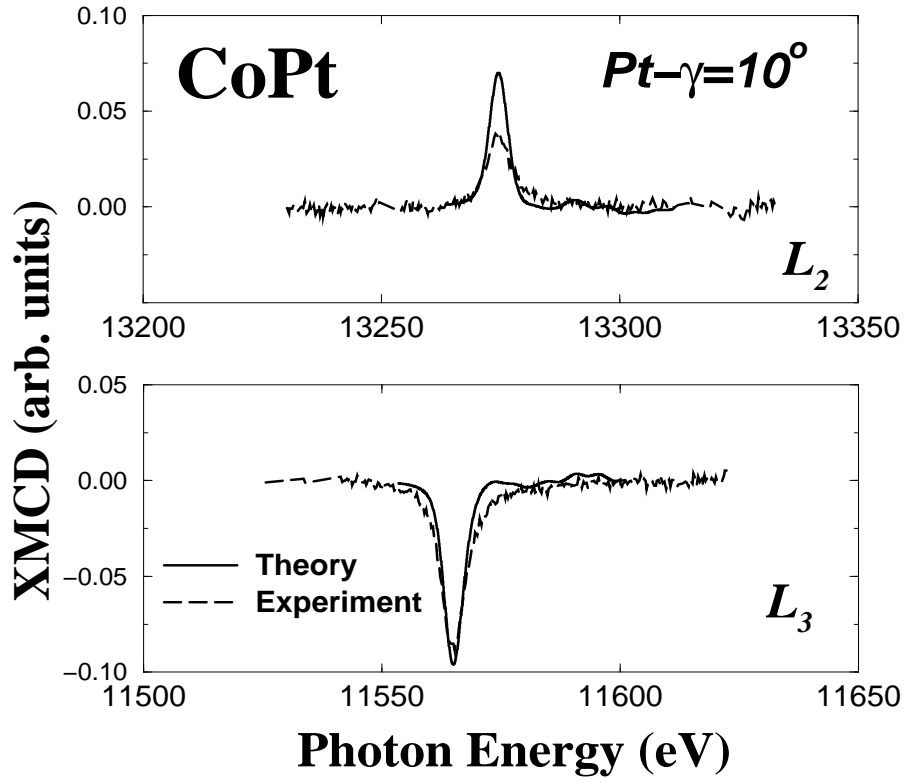


FIG. 9. Calculated and experimental platinum XMCD spectra at L_2 and L_3 edges for $\gamma=10^\circ$ in the CoPt compound (γ is the angle between the [001] direction and the spin quantization axis). The agreement between the theory and the experiment is better than in the case of cobalt because the core hole is deeper.

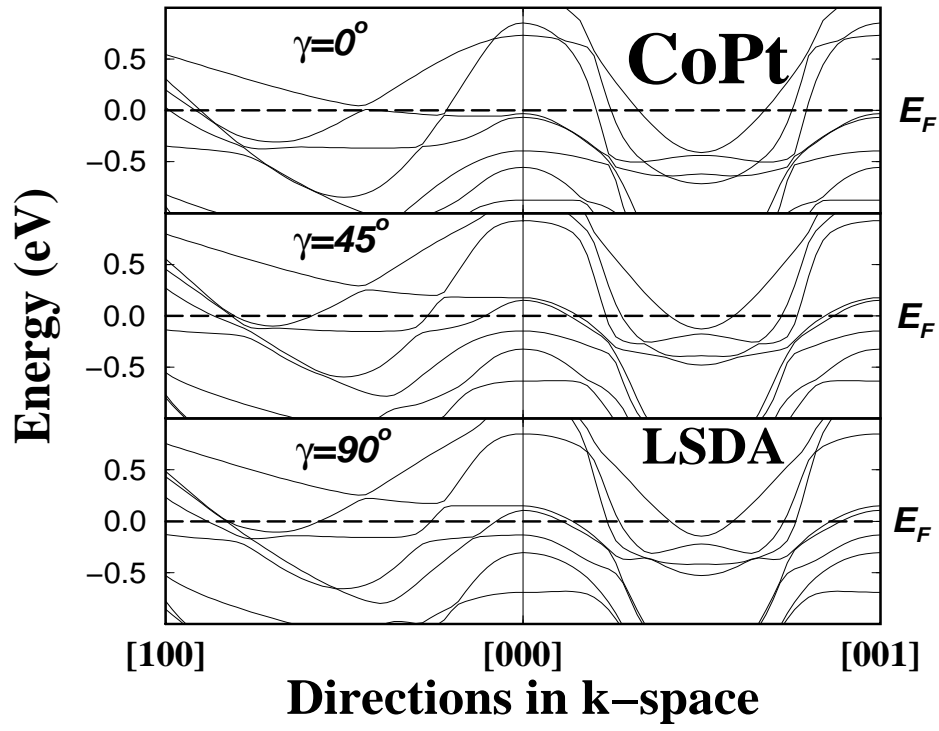


FIG. 10. CoPt band structure around the Fermi level along two high symmetry directions of the Brillouin zone as a function of the angle γ between the [001] direction and the spin quantization axis.

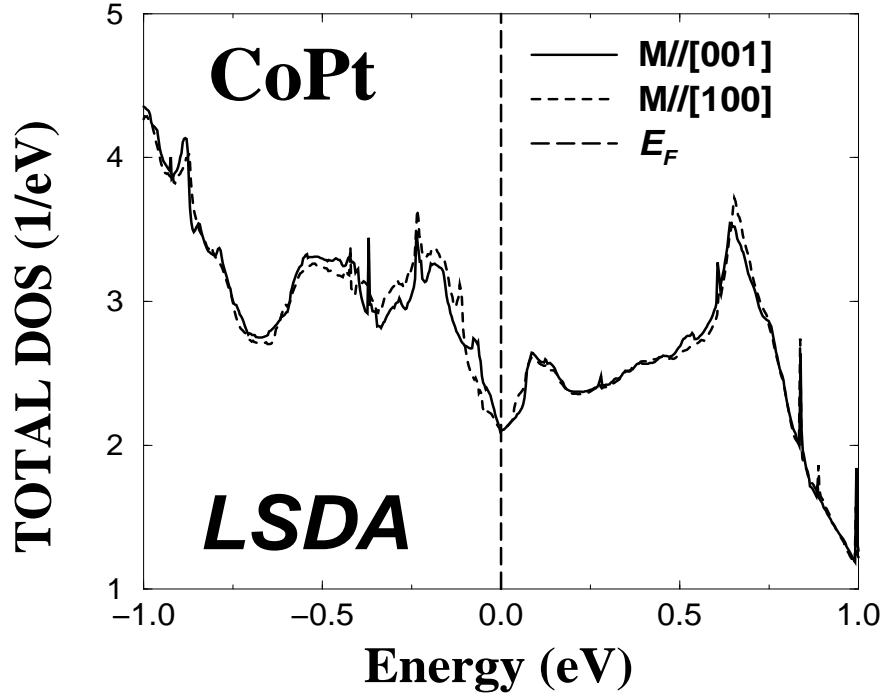


FIG. 11. Total density of states for CoPt at the vicinity of the Fermi level, for the spin quantization axis along the [001] and [100] magnetization axis. The states just below the Fermi level suggest that the hard axis is favored which led as to conclude that the MCA is due to the changes in all the DOS.